Applied Catalysis B: Environmental 129 (2013) 426–436

Contents lists available at SciVerse ScienceDirect

Applied Catalysis B: Environmental

journal homepage: www.elsevier.com/locate/apcatb

Liquid–solid heterogeneous synthesis of highly dispersed and PdPt surface enriched PdPtCu/C as methanol tolerant oxygen reduction reaction catalysts

Wei Li, Xinsheng Zhao, Thomas Cochell, Arumugam Manthiram*

Materials Science and Engineering Program and Texas Material Institute, The University of Texas at Austin, Austin, TX 78712, United States

ARTICLE INFO

Article history:
Received 30 May 2012
Received in revised form
18 September 2012
Accepted 27 September 2012
Available online 5 October 2012

Keywords:
Platinum palladium copper alloy
Heterogeneous synthesis
Surface enrichment
Oxygen reduction reaction
Methanol tolerance

ABSTRACT

We present a liquid–solid heterogeneous synthesis with switchable etching effects to prepare highly dispersed, PdPt surface enriched PdPtCu alloy nanoparticles (NPs) supported on carbon black (PdPtCu/C) by using Cu NPs as a heterogeneous reducing agent. A mixture of the Pd and Pt precursors and nanosized particles of Cu are required to form the highly dispersed PdPtCu alloy NPs and scatter them on the carbon black. Oxidative etching of the surface Cu with the reaction solution triggered by switching the reaction solution atmosphere from N_2 to air results in an enrichment of the surface of PdPtCu by PdPt. The activity towards the oxygen reduction reaction and methanol tolerance is tuned by controlling the Pd/Pt ratio. The PdPtCu/C catalyst with a Pd/Pt molar ratio of 1:1 exhibits noble metal and Pt mass activities of, respectively, 2 and 3 times that of a commercial Pt/C at 0.85 V vs. RHE with much superior methanol tolerance. It also shows better performance than Pt/C with comparable durability in a direct methanol fuel cell.

1. Introduction

Low-temperature fuel cells (LTFCs) are attractive for the applications as portable and transportation power sources mainly due to the low operational temperature [1]. However, the continuing development of the LTFC technology needs to reduce the cost and improve both the activity and selectivity of the-state-of-art catalysts, i.e. Pt nanoparticles (NPs) on carbon black support (Pt/C). Alloying of Pt with less expensive metals is a promising way to address these challenges. On the other hand, Pd is of interest as it is less expensive than Pt, stable in the acidic fuel cell environment, and has attractive electrocatalytic properties: highest electrocatalytic activity toward both hydrogen oxidation reaction (HOR) and oxygen reduction reaction (ORR) in acidic media among the pure metals with the exception of Pt [2], high activity toward CO electrooxidation [3–13], and little electrocatalytic activity toward alcohol oxidation in acidic media [14].

To date, carbon-supported PdPt bimetallic NPs with different Pd/Pt ratios and structures (PdPt/C) have been reported as promising electrocatalysts with lower cost and higher activity and selectivity compared to Pt/C catalysts for HOR [15], methanol oxidation reaction (MOR) [3–6], ethanol oxidation reaction (EOR) [5,7,8], formic acid oxidation reaction (FAOR) [9–13], and ORR [16–18] in LTFCs. Such capability of PdPt NPs for diverse reactions is accredited to synergistic effects (ensemble effect [19], ligand effect [19], and strain effect [20]) between Pd and Pt arising from the various compositions and structures [3–13,15–18,21]. To further reduce the cost and increase the noble metal based activities of the PdPt catalysts, Cu, an inexpensive and relatively stable transition metal in acidic media, has been added to develop PdPtCu ternary metallic catalysts [22–26]. Typically, the PdPtCu ternary metallic nanoparticles have Cu or PdCu in the core, and Pt or PdPt in the shell [22–26]. Because Cu has a smaller lattice parameter (fcc structure) compared to Pd and Pt, the addition of Cu into the core results in a compressive strain on the Pt or PtPd in the shell, leading to a slight downshift of the Pt d-band center and a weakening of the chemisorption of oxygen-containing species that enhances the ORR activity of Pt [25].

PdPt, PdCu, and PdPtCu alloy NPs are usually synthesized by solution-based chemical routes with reducing agents dissolved in the reaction solutions [4,7–9,15,16,27–30]. There are very few reports of using a non-dissolved solid as a heterogeneous reducing agent to prepare metal NPs in a solid–liquid two-phase system [31–33]. Wu and Zeng [31,32] used Fe and Cu foils to prepare noble metal (Au and Pt) NPs with the assistance of ultrasonication and hydrodynamic forces. Wen et al. [33] synthesized dendritic nanostructures of silver by using zinc microparticles. These heterogeneous reduction reactions are galvanic replacement reactions, which are based on the redox reaction principle, i.e., a metal ion or ion complex can be reduced to a corresponding atomic state in solution by another metal with a relatively lower reduction potential [31–33]. The heterogeneous reactions occur at the interface of the solid and the liquid, and are generally employed to build

* Corresponding author. Tel.: +1 512 471 1791; fax: +1 512 471 7681.
E-mail address: rmanth@mail.utexas.edu (A. Manthiram).

0926-3373/$ – see front matter © 2012 Elsevier B.V. All rights reserved.
http://dx.doi.org/10.1016/j.apcatb.2012.09.044

a core-shell structure or decorate the core for the bimetallic and ternary metallic catalysts, such as carbon-supported core-shell structures of PdCu@Pt [22] and Pt-decorated PdCu alloy NPs [26]. These types of architectures with engineered nanoscale surfaces increase the activity and stability of the catalysts with significant reductions in the use of noble metals. Constructing such catalyst architectures is thus the most promising way to address the issues of high cost and low activity and selectivity for LTFCs. To the best of our knowledge, there are no reports in the literature to use the galvanic replacement reactions only to heterogeneously synthesize alloy NPs with controlled compositions and architectures.

Accordingly, we present here a new facile route using Cu NPs as solid heterogeneous reducing agents to synthesize highly dispersed, PtPd-surface-enriched PdPtCu ternary alloy NPs supported on carbon black with varied compositions as cathode catalysts for direct methanol fuel cells (DMFCs), a promising type of LTFCs. These catalysts should have high ORR activity with superior methanol tolerance to address one of the major issues of DMFCs, i.e., methanol crossover from the anode to the cathode through the membrane. This crossover poisons the Pt cathode catalysts and causes a "mixed potential", leading to dramatic performance losses [34,35]. The structure, composition, and morphology of the as-prepared PdPtCu/C catalysts have been characterized by various physical and electrochemical techniques. The influence of the Pd/Pt ratio on ORR activities in the absence and presence of methanol is discussed for the prospective usage of this synthesis route for preparing catalysts for other reactions in LTFCs.

2. Experimental

2.1. Synthesis of catalysts

The carbon-supported copper (Cu/C) was prepared by a reduction of the copper acetate (monohydrate, ACS, Alfa Aesar) with L-(+)-ascorbic acid (ACS, Alfa Aesar) in ethylene glycol (EG, ACS, Fisher Scientific). Afterward, a mixture of Na_2PdCl_4/K_2PtCl_4 (anhydrous, Alfa Aesar) in EG was added to synthesize the PdPtCu/C catalyst with the reduction reactions occurring between the Cu and the $[PdC1_4]^{2-}$/$[PtC1_4]^{2-}$ ions. Typically, a mixture of 0.70 mmol copper acetate and 150 mg carbon black (Vulcan XC-72R, Cabot) was dispersed in 45 mL of EG at 60 °C by sonication for 30 min followed by vigorous stirring for 2 h in sequence. The dispersion was then deaerated with N_2 (UHP, Airgas) for 30 min. Next, an ascorbic acid/EG solution (0.25 mol L^{-1}, 0.74 mmol) was added dropwise to the dispersion and the reduction reaction continued for 30 min at 60 °C under vigorous stirring and N_2 shield. Afterward, a mixture of Na_2PdCl_4/K_2PtCl_4 in EG (0.03 mol L^{-1}, 0.63 mmol) with a certain Pd/Pt molar ratio was added dropwise and the reduction reactions continued at 60 °C for 3 h with the shield of N_2. The reaction solution was then cooled to room temperature and kept stirring with exposure to air overnight to etch the residual Cu exposed to the solution. The PdPtCu/C catalyst formed was filtered, washed with deionized water (4 mL water per mg of catalyst), and dried in a vacuum oven overnight. In this study, four PdPtCu/C catalysts were prepared with the Na_2PdCl_4/K_2PtCl_4 molar ratios of 85:15, 75:25, 50:50, and 25:75, which are hereafter denoted as, respectively, PdPtCu/C-$Pd_{85}Pt_{15}$, PdPtCu/C-$Pd_{75}Pt_{25}$, PdPtCu/C-$Pd_{50}Pt_{50}$, and PdPtCu/C-$Pd_{25}Pt_{75}$. PdCu/C and PtCu/C were also synthesized using the same procedures and conditions for a comparison.

2.2. Physical characterizations

Powder X-ray diffraction (XRD) patterns of the samples, recorded on a Philips APD 3520 diffractometer with Cu Kα radiation (λ = 0.15418 nm), were processed and analyzed with the JADE 9.0 software package (Rigaku). The compositions of the samples were obtained with the energy-dispersive X-ray spectroscopy (EDS) analysis carried out on a JEOL-JSM5610 SEM equipped with an EDS attachment (Oxford instruments). INCA software (Oxford instruments) was used to quantify the EDS spectra, employing the XRP correction method for matrix corrections. PdPt NPs with different compositions prepared using $NaBH_4$ as the reducing agent were utilized as the standards to get a calibration curve for the EDS quantitative analysis. X-ray photoelectron spectroscopy (XPS) characterization was performed with a Kratos Axis Ultra DLD photoelectron spectrometer (Shimadzu) equipped with a monochromatic Al Kα X-ray source. The XPS peaks were fitted and analyzed with CasaXPS software (version 2.3.1.4, Casa Software). The doublet peaks were fitted with a Shirley-type background, a 30% Gaussian-Lorentzian function, and three constraints on the component peaks: the position (3.33 eV between Pt $4f_{7/2}$ and Pt $4f_{5/2}$, 5.3 eV between Pd $3d_{5/2}$ and Pd $3d_{3/2}$), the peak area ratio ($d_{5/2}$:$d_{3/2}$ = 3:2, $f_{7/2}$:$f_{5/2}$ = 4:3), and equal full width at half maximum. The transmission electron microscopy (TEM) images were acquired with a JEOL 2010F transmission electron microscope operated at 200 keV to characterize the morphology of the samples. The particle size distributions were obtained from the TEM images by using ImageJ software (NIH). The metal loadings of the samples were determined by burning off the carbon support in air at 500 °C for 1.5 h, followed by the verification of the oxidation states of the residual materials by XRD. To obtain good reproducibility and minimal errors, an aluminum foil crucible and about 50–100 mg sample were employed.

2.3. Electrochemical measurements

The electrochemical experiments were carried out on a potentiostat (Autolab PGSTAT302N, Eco Chemie B.V.) with a three electrode configuration: a Pt mesh as the counter electrode, a glassy carbon rotating disk electrode (RDE, 5 mm diameter, Pine instrument) as the working electrode, and a saturated calomel electrode as the reference electrode. All potentials in this study are reported against the reversible hydrogen electrode (RHE).

Before each experiment, the RDE with a mirror-finished surface was polished with 0.05 μm γ-alumina micropolish (Buehler) on a microcloth PSA (Buehler) for 1 min, and then washed by rinsing and ultrasonication (30 s) with deionized water three times to obtain a clean, fresh surface. Catalyst ink (2.0 mg_{cat} mL^{-1}) was prepared by dispersing the catalyst in a 3:1 (v/v) deionized water/isopropanol mixture by sonication for 15 min. A 6.0 μL aliquot of the ink was casted onto the RDE to give a loading of 24.5 μg_{metal} cm^{-2} with a syringe (10 μL, Hamilton) and dried at room temperature.

Cyclic voltammetry experiments were conducted in a N_2 saturated 0.10 M $HClO_4$ (ultrapure, Optima*, Fisher Scientific) electrolyte. The working electrode potential was cycled 20 times between 0 and 1.2 V at a scan rate of 100 mV s^{-1} to clean the catalyst surface. The stable cyclic voltammograms between 0 and 1.0 V at a scan rate of 20 mV s^{-1} obtained after the cleaning process are reported here.

Thereafter, the catalyst-coated RDE was mounted onto an interchangeable RDE holder (Pine Instruments) and immersed in an O_2 (UHP, Airgas) saturated 0.10 M $HClO_4$ in a 150 mL five-neck electrochemical cell for rotating electrodes (AFCELL3, Pine Instrument). The hydrodynamic voltammetry experiments were performed with a rotation rate of 1600 rpm and a linear potential sweep from 0.1 to 1.0 V at a scan rate of 20 mV s^{-1}. The obtained polarization curves were used to determine the ORR activities of the samples. Methanol tolerance was measured under the same conditions in a mixture of 0.1 M $HClO_4$ and 0.1 M methanol (Optima*, Fisher Scientific).

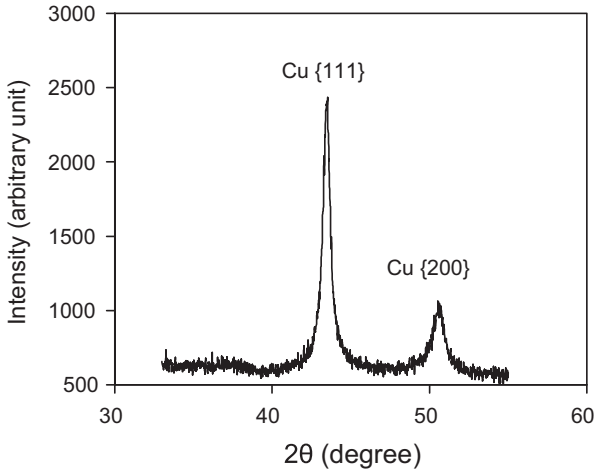

Fig. 1. XRD pattern of Cu/C prepared with a 1.05:1 molar ratio of ascorbic acid to copper.

2.4. MEA fabrication and testing in a DMFC single cell

The membrane electrode assembly (MEA) fabrication and testing in a direct methanol fuel cell (DMFC) single cell are briefly described as follows. Further details can be found in a previous publication [36].

Two 5 cm^2 square MEAs (PdPtCu/C-$Pd_{50}Pt_{50}$ and Pt/C) were fabricated by hot-pressing a piece of Nafion® 115 membrane (DuPont) between the two electrodes (anode and cathode) at 130 °C under a pressure of 50 kg cm^{-2} for 3.0 min. The PdPtCu/C-$Pd_{50}Pt_{50}$ MEA has anode and cathode loaded, respectively, with 2.5 mg_{metal} cm^{-2} commercial PtRu/C (40 wt% Pt and 20 wt% Ru, Johnson Matthey) and 2.5 mg_{metal} cm^{-2} PdPtCu/C-$Pd_{50}Pt_{50}$ (33 wt% Pd + Pt, homemade). The Pt/C MEA has the same anode but a different cathode with 2.5 mg_{metal} cm^{-2} Pt/C (40 wt%, Johnson Matthey, denoted as Pt/C (JM)). The mass ratio of dry Nafion ionomer (EW1000, Dupont) to carbon was fixed at 0.8.

The MEA was then assembled in a 5 cm^2 single cell hardware (Electrochem) consisting of two graphite plates with serpentine channels for testing on a fuel cell test station (850 C, Scribner). An aqueous methanol solution (2 mol L^{-1}, 1.0 mL min^{-1}, room temperature) and humidified O_2 (200 mL min^{-1}, 65 °C) were fed, respectively, to the anode and the cathode. The polarization curves of the MEA at 65 °C without backpressure were recorded potentiostatically on the electronic load bank in the test station.

3. Results and discussion

3.1. Synthesis and mechanisms to form highly dispersed PdPtCu NPs loaded on carbon support

The carbon-supported copper (Cu/C) was synthesized by reducing copper acetate with ascorbic acid in EG at 60 °C in a N_2 atmosphere. When the molar ratio of ascorbic acid to copper is equal to and larger than 1.05, pure metallic phase Cu is obtained as confirmed by the XRD pattern in Fig. 1. Required amounts of the precursor solutions of Na_2PdCl_4 and/or K_2PtCl_4 were then added to prepare PdCu/C, PtCu/C, and PdPtCu/C. The preparation of metallic Pd and Pt by the replacement reactions between Cu and Pd/Pt precursors, i.e. Na_2PdCl_4/K_2PtCl_4, is thermodynamically favorable according to their redox standard potential as follows [37]:

$$[PtC1_4]^{2-} + 2e^- = Pt + 4C1^-; \quad E^\circ = 0.755\,V \tag{1}$$

$$[PdC1_4]^{2-} + 2e^- = Pd + 4C1^-; \quad E^\circ = 0.591\,V \tag{2}$$

$$Cu^{2+} + 2e^- = Cu; \quad E^\circ = 0.342\,V \tag{3}$$

Accordingly, the $[PdC1_4]^{2-}$ and $[PtC1_4]^{2-}$ can be reduced, respectively, to metallic Pd and Pt:

$$2Cu + [PdCl_4]^{2-} \rightarrow 2Cu^{2+} + 4Cl^- + Pd \tag{4}$$

$$2Cu + [PdC1_4]^{2-} \rightarrow 2Cu^{2+} + 4Cl^- + Pt \tag{5}$$

Although the Cu NPs aggregate on the carbon black (Fig. 2a), highly dispersed and narrowly distributed PdPtCu NPs were formed through the replacement reactions between the Cu NPs and the Pd/Pt precursors (Pd:Pt = 2:1) in EG at 60 °C, and the NPs were uniformly loaded on the carbon support, as shown in Fig. 2b. Unlike the conventional liquid–liquid reduction reactions, the solid–liquid heterogeneous reduction reactions take place in the interface between the solid (the aggregated Cu NPs as the reducing agent) and the liquid (the reaction solution containing the metal complexes of $[PdC1_4]^{2-}/[PtC1_4]^{2-}$). The reduced PdPt atoms and clusters/nuclei have intermolecular forces with the aggregated Cu NPs and solvent molecules. When the latter is larger than the former, they leave the surface of Cu NPs and go into the solution, where they grow up or deposit back on the carbon black and then grow up to NPs. This is different from that using a Cu foil, in which the noble metal clusters accumulate on the foil [31,32], indicating stronger intermolecular forces between the bulk Cu atoms and the noble metal clusters than that between the surface Cu atoms on NPs and the noble metal clusters. During this process, the Cu atoms or clusters could be incorporated into the PdPt clusters to form PdPtCu alloy NPs, which will be discussed in detail in Section 3.2.

There is an interesting finding that the prepared PtCu NPs on the carbon black have severe aggregation with a small particle size of around 3 nm while the PdCu NPs have a larger particle size of about 10–40 nm, as shown in Fig. 2c and d. These opposite results compared to that of PdPtCu NPs imply that synergistic effects exist between Pd and Pt to mitigate particle size increases and aggregation of the NPs. The inclination for Pd clusters to detach from the Cu NPs indicates weaker intermolecular forces between the Pd clusters and Cu NPs. The detached Pd clusters grow up to large particles because of the low free surface energy of Pd (2.003 J m^{-2} for Pd (1 1 1) [38]). On the contrary, the Pt NPs have small particle sizes owing to its large surface energy (2.489 J m^{-2} for Pt (1 1 1) [38]). The aggregation of PtCu NPs suggests that the Pt clusters are inclined to stay on the surface of Cu due to stronger intermolecular forces between the Pt clusters and Cu NPs. This certainly means that the Pt clusters nucleate on the surface of the Cu NPs. When Pd and Pt precursors are co-reduced by Cu NPs, the formed PtPd clusters have an intermediate surface energy and affinity with Cu compared to pure Pd or Pt. As a result, highly dispersed and narrowly distributed PdPtCu NPs on the carbon black support are obtained. We have confirmed that the synergistic effects contribute significantly to the high dispersion of PdPtCu NPs when the content of Pd or Pt is as low as 10 at.%. The four as-prepared catalysts, PdPtCu/C-$Pd_{85}Pt_{15}$, PdPtCu/C-$Pd_{75}Pt_{25}$, PdPtCu/C-$Pd_{50}Pt_{50}$, and PdPtCu/C-$Pd_{25}Pt_{75}$, have mean particle diameters of 3.69, 3.83, 3.62, and 3.63 nm, respectively, measured from the TEM images in Fig. 3. The four catalysts also have the same standard deviation of 0.83 nm except for PdPtCu/C-$Pd_{75}Pt_{25}$, which is 0.74 nm. This demonstrates that highly dispersed carbon-supported PdPtCu catalysts with narrow particle size distributions were formed. Moreover, the mean particle diameters and standard deviations are very close to those of Pt/C (JM), which are 3.79 nm and 0.91 nm, respectively, in Fig. 3e. The similarity of the mean particle sizes and the distributions means that the particle size effects on electrochemical evaluation are negligible.

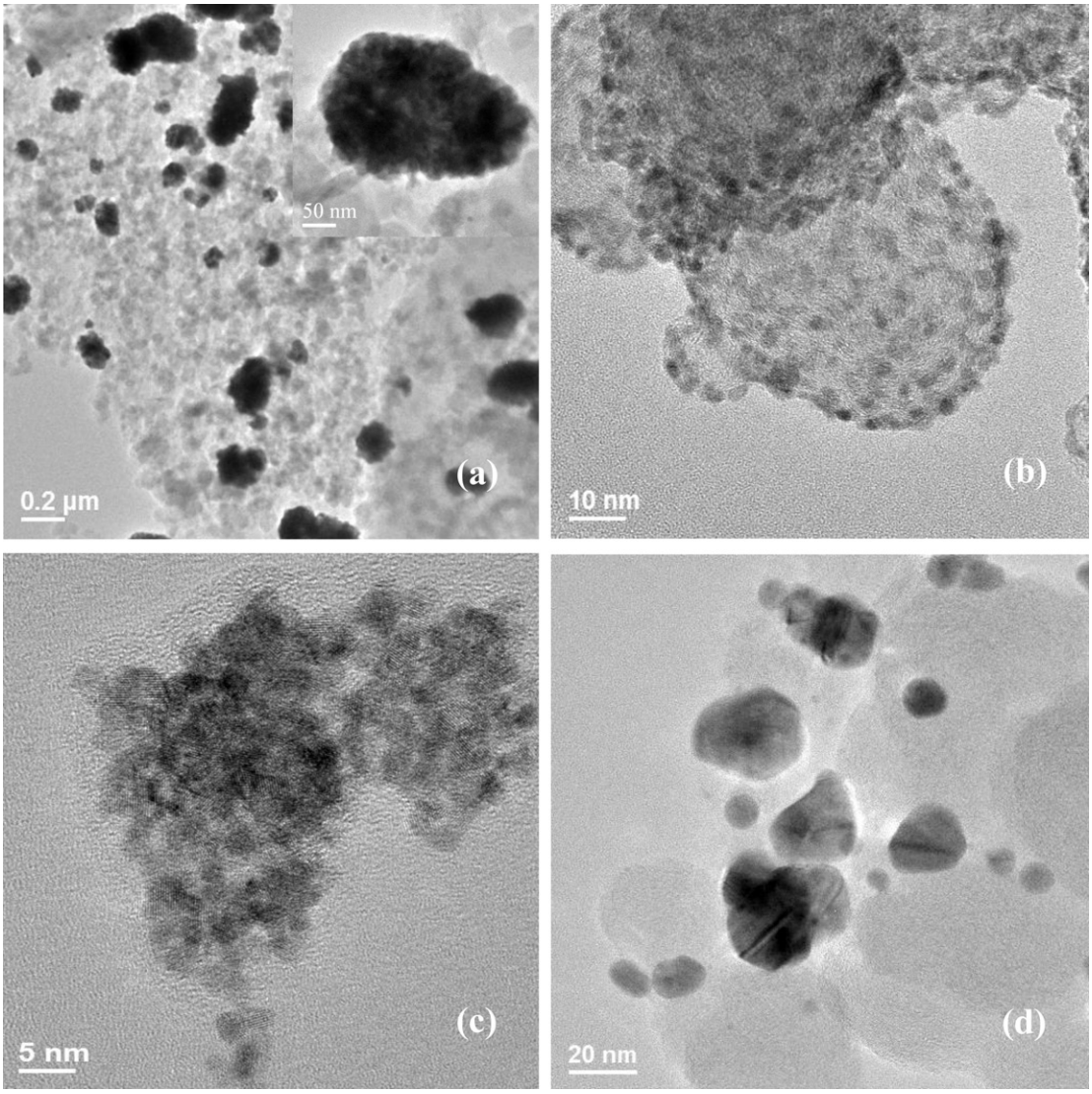

Fig. 2. TEM images of (a) Cu/C, (b) PdPtCu/C, (c) PtCu/C, and (d) PdCu/C.

3.2. Composition and structure

All the samples were synthesized at 60 °C for 3 h. Certainly, the synthesis could be carried out at a higher temperature, where the EG works as another reducing agent. This is not desirable for this study on using Cu NPs as a reducing agent and should be avoided. Fig. 4 shows the atomic percentages of Pt and Cu in the samples against the Pt atomic percentage in the precursors. It can be seen that the compositions of the PdPt in the PdPtCu/C catalysts were readily tuned, but the Pt/Pd molar ratios in the synthesized samples were slightly lower than the nominal values in the case of samples with Pt/Pd ratio > 1. The composition determination with EDS was calibrated with the PdPt NPs prepared using $NaBH_4$ as reducing agent, which has strong reducing capability and reduces the Pd/Pt precursors completely as shown by the calibration curve in the inset of Fig. 4.

As mentioned in Section 3.1, the standard potential of $[PtC1_4]^{2-}$/Pt is higher than that of $[PdC1_4]^{2-}$/Pd, suggesting that the replacement reactions of Cu with K_2PtCl_4 should be thermodynamically more favorable than that with Na_2PdCl_4. Moreover, a controlled experiment without carbon black shows that the solutions of K_2PtCl_4/EG and Na_2PdCl_4/EG turn black in about 1 min and 5 min, respectively, after the addition of Cu NPs at room temperature, demonstrating that the former replacement reaction is faster. Both control experiments would imply that the Pt/Pd molar ratios should not be lower than those in the precursors, i.e. the replacement reaction of K_2PtCl_4 with Cu should have higher conversion than that of Na_2PdCl_4 with Cu. The contrary experimental result could be accredited to the stronger interaction between Pt and Cu discussed in Section 3.1, which makes the reduced Pt atoms and clusters be inclined to stay on the Cu surface to protect the inside Cu atoms from reduction and brings about a lower conversion compared to that of Pd. The stronger interaction between Pt and Cu causes more Cu atoms incorporated into the PdPt clusters and finally into the NPs. It is supported by the increase of the atomic percentage of Cu in the samples as the Pt percentage increases, as seen in Fig. 4.

The fast replacement reactions between Cu NPs and K_2PtCl_4/Na_2PdCl_4, i.e. the solutions of K_2PtCl_4 and Na_2PdCl_4 turn black immediately after the addition of Cu NPs at 60 °C, make it possible to produce the alloy nanoparticles of PdPtCu. Fig. 5a shows the XRD patterns of those PdPtCu/C samples, in which all the patterns have a single fcc structure with four diffraction peaks corresponding to (1 1 1), (2 0 0), (2 2 0), and (3 1 1), with their positions shifting to higher 2-theta values compared to those of Pt

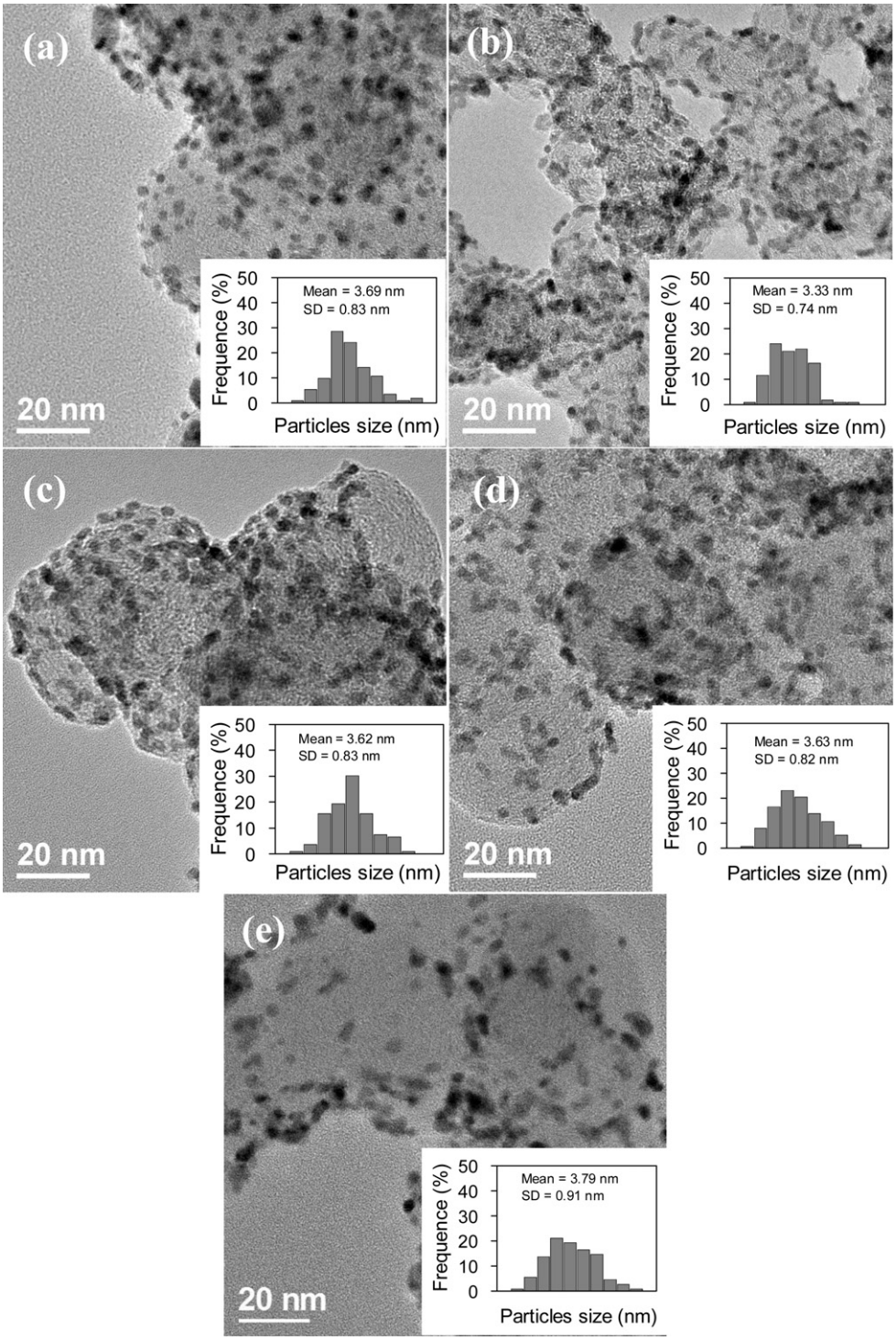

Fig. 3. TEM images of PdPtCu/C samples with the molar ratio of Pd to Pt: (a) 85:15, (b) 75:25, (c) 50:50, and (d) 25:75, as well as (e) Pt/C (40 wt%, JM).

and Pd. Moreover, the 2-theta shifting increases as the Pt content increases, with which Cu content increases as shown in Fig. 4. This evidence suggests the alloying of Pd, Pt, and the residual Cu.

The Cu in the surface layer of the PdPtCu NPs was removed by the etching effect from the reaction solution. It was illustrated by the disappearance of the Cu^{2+}/Cu redox peaks located in the range of 0.4–0.6 V [24] of the cyclic voltammograms (CVs) for PdPtCu/C-$Pd_{75}Pt_{25}$ before and after etching in Fig. 6. We also confirmed the etching effect by a controlled experiment, in which the prepared Cu NPs on carbon black can be completely dissolved in the reaction solution, as shown in Fig. S1. It is well known that Cu^{2+} catalyzes the oxidation of ascorbic acid with O_2 [39,40]. In this study, the ascorbic acid was only 10% more than the stoichiometric amount required to reduce the copper acetate. Thus, a small amount of Cu^{2+} may exist due to the existence of reverse reaction (Cu oxidation reaction). When the reaction solution is exposed to air, the oxidation of ascorbic acid starts, which pushes the reduction reaction of copper acetate to the reversed side and thus more Cu^{2+} appears. Moreover, the Cu^{2+} in the acidic reaction solution has oxidative capability to etch the Cu [41,42]. Therefore, the etching of copper is triggered by

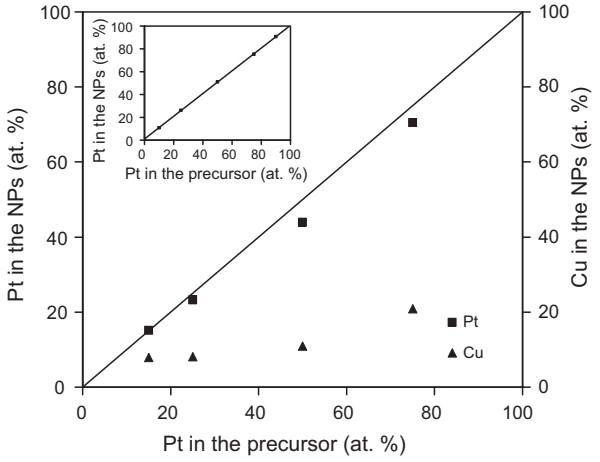

Fig. 4. Atomic percentages of Pt and Cu in the nanoparticles (NPs) as determined by EDS against the Pt atomic percentage in the precursors. The Pt at.% values are based on the Pt and Pd contents only while the Cu at.% values are based on the Pt, Pd, and Cu contents. The inset is the calibration curve for EDS using the PdPt NPs prepared by applying $NaBH_4$ as the reducing agent.

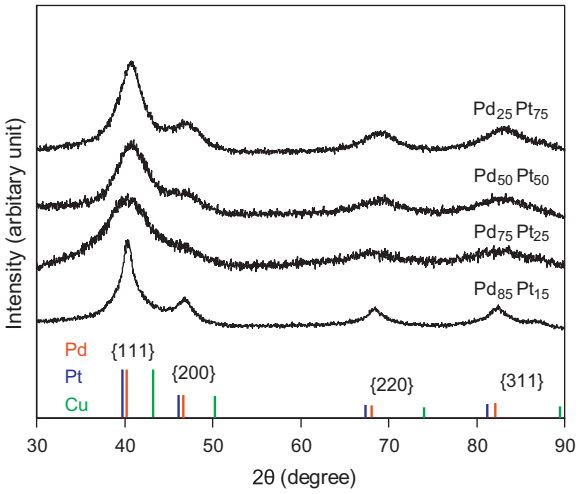

Fig. 5. XRD patterns of the PdPtCu/C samples with different Pd/Pt molar ratios.

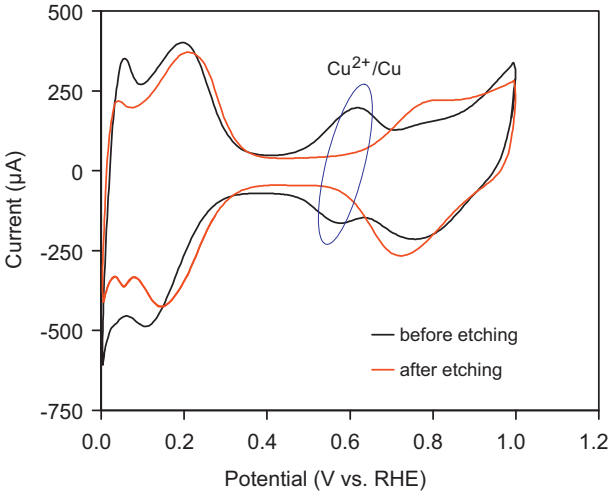

Fig. 6. CVs of PdPtCu/C-$Pd_{75}Pt_{25}$ (a) before etching and (b) after etching.

the introduction of air and then accelerated with the appearance of more Cu^{2+}. After the replacement reactions, the reaction solution has higher Cu^{2+} concentration than in the controlled experiment, and thus the etching rate is faster in the preparation of PdPtCu/C. The Cu in the surface layer of the PdPtCu NPs is removed by this etching effect, leaving the surface enriched with PdPt, which was confirmed by cyclic voltammetry data discussed later in this section. Below the surface, metallic Cu exists, as indicated by the XPS Cu 2p spectra in Fig. S2, which is covered by PdPt and protected from the etching.

Fig. 7a and b show, respectively, the Pd 3d and Pt 4f XPS spectra of the PdPtCu/C samples. Because Na_2PdCl_4 and K_2PtCl_4 were used as precursors, +4 valence Pd and Pt components were not considered for peak fitting. The Pd 3d spectra of PdPtCu/C-$Pd_{25}Pt_{75}$ and PdPtCu/C-$Pd_{50}Pt_{50}$ have Pt $3d_{3/2}$ peaks located between 330 and 335 eV due to high Pt contents. As a result, the Pt $3d_{3/2}$ peak of PdPtCu/C-$Pd_{25}Pt_{75}$ has a significant contribution to the adjacent Pd 3d peaks, so it was considered in the peak fitting without the constraints mentioned in the experimental part. However, the Pt $3d_{3/2}$ peak of PdPtCu/C-$Pd_{50}Pt_{50}$ at 330–335 eV was ignored in the peak fitting because of its negligible contribution. Fig. 7c compares the percentages of Pd and Pt oxides in the PdPtCu/C samples determined from the XPS spectra in Fig. 7a and b. First, it shows that large amounts of Pd and Pt oxides were formed in all samples. However, the XRD patterns in Fig. 5 do not show any peaks corresponding to oxides, which suggests that the oxidation occurs at the near surface region of the samples and cannot form enough reflections to generate diffraction peaks or the oxides are amorphous. Although bulk noble metals (Pt and Pt in this study) are resistant to being oxidized, their NPs are subject to oxidation at their surface in air at room temperature [43]. The percentages of Pd and Pt oxides are rather high because the samples were stirred in the reaction solution exposed to air overnight to remove Cu. As previously stated, the solution has a strong oxidative capability since it can oxidize Cu NPs to Cu ions. Pd has a higher percentage of oxide compared to Pt because Pd is more thermodynamically prone to oxidation due to a lower standard reduction potential.

The composition-dependent electrochemical behaviors of the PdPt surface enrichment and alloy structure of PdPtCu were also characterized. CVs of the Pd/C, PdPtCu/C, and Pt/C (JM) in N_2 saturated 0.1 M $HClO_4$ are presented in Fig. 8. Significant differences in the hydrogen region (0–0.4 V vs. RHE) of the CVs can be observed. Pd/C has two typical types of hydrogen waves: sharp hydrogen peaks mainly from the absorption/desorption processes of the hydrogen absorption (H_{abs}) located in the lower hydrogen region and broad peaks from the adsorption/desorption processes of underpotential deposition hydrogen (H_{UPD}) in the higher hydrogen region [44–46]. As the Pt content increases up to 50 at.%, the H_{abs} of Pd decreases and also shifts to a lower potential. The H_{abs} of Pd eventually disappears when the Pt content is above 50 at.%. On the other hand, Pt has three H_{UPD} peaks related to the three facets: (1 1 1), (1 1 0), and (1 0 0), located at 0.13, 0.18, and 0.27 V, respectively [47]. As the Pd content increases in the PdPtCu/C samples, the alloyed Pd modifies the Pt surface structure or facets, causing the disappearance of the three H_{UPD} peaks of Pt.

Similarly, the surface composition and structure changes were also characterized by the changes of the oxygen waves in Fig. 8. It is hard to use the anodic waves of Pd or Pt for characterization because they are complicated and do not have resolved peaks and obvious onset potentials [48–50]. However, the cathodic waves have well resolved reduction peaks, which can be used to characterize the composition and structure changes of the surface. It has been reported that the oxidation of Pd forms PdO, not PdOH, which has an onset potential of about 0.7 V and approaches a monolayer on Pd at 1.4 or 1.5 V [51,52]. Pt, on the other hand, is first oxidized to PtOH at about 0.9 V and forms a PtOH monolayer on Pt at 1.1 V [49]. As the

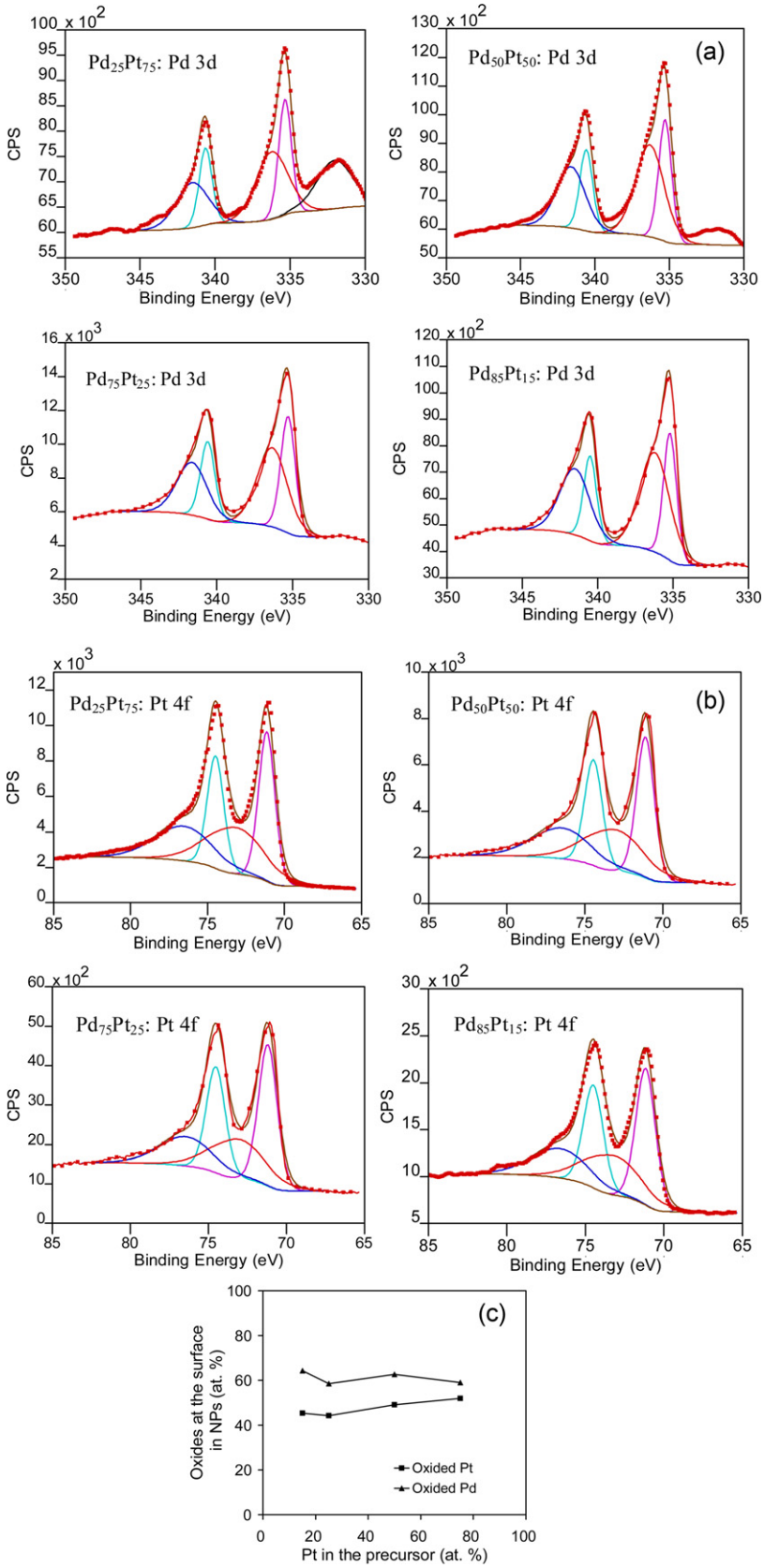

Fig. 7. XPS spectra of the PdPtCu/C samples with different Pd/Pt molar ratios: (a) Pd 3d and (b) Pt 4f; (c) surface oxides of those samples determined by XPS. The at.% values are based on the Pt and Pd contents only.

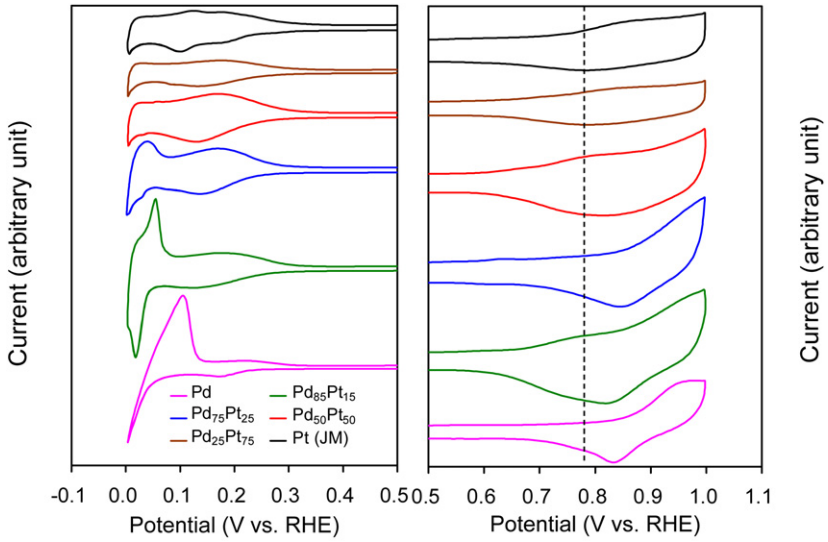

Fig. 8. CVs of the PdPtCu/C samples with different Pd/Pt molar ratios and commercial Pt/C (JM) in N_2 saturated 0.1 M $HClO_4$ at room temperature with a scan rate of 20 mV s^{-1} in the range of 0–1.0 V vs. RHE.

potential further increases, the PtOH is oxidized to PtO and then to PtO_x [49]. In this study, PtOH and PdO exist as a sub-monolayer on Pt and Pd, respectively, because the higher limit of potential cycling of 1.0 V is lower than the potentials required to form a monolayer. Pt/C (JM) has the reduction peak located around 0.78 V as shown in Fig. 8. As the Pd content of the PdPtCu/C catalysts increases, the reduction peaks shift to a higher potential. This confirms that Pd and Pt are closely associated with each other, i.e. form an alloy, at the surface of the PdPtCu.

3.3. Composition dependent activities toward ORR and methanol tolerance

As discussed above, the PdPtCu/C catalysts are PdPt surface enriched and their composition dependent performances are thus discussed based on the Pd/Pt ratio. The electrochemically active surface area (ECSA) of the PdPtCu/C catalysts cannot be obtained based on the analysis of the H_{UPD} waves of CVs because of the strong H absorption of Pd beneath the surface [44–46]. Thus the activity should be normalized to the mass (mass activity) for comparison. The real metal loadings of PdPtCu/C were determined by burning off the carbon black in air at 500 °C for 1.5 h, and are shown in Table 1. Complete removal of the carbon black support was confirmed by two results: no mass change after heating the residual materials for one more hour and the residual materials dissolved completely in 1 M HCl when the catalysts do not contain Pt. XRD confirmed that the residual materials consist of CuO, PdO [53], and Pt. The metal loadings of Pd and Pt were thus calculated based on the mass change after the burn off and the molar ratio of Cu, Pd, and Pt were determined by EDS.

Fig. 9a compares the hydrodynamic polarization curves of the PdPtCu/C catalysts with different Pd/Pt molar ratios and Pt/C (JM). All the catalysts have diffusion-limiting currents of 6.0 ± 0.3 mA cm^{-2}. The slight discrepancy of the limiting currents is attributed to the different geometric areas of the catalyst coatings on the RDE due to minor casting inconsistencies. It affects the curves in the mixed regions of kinetics and diffusion, but not in the kinetic region, where the kinetics dominates the measured currents [54]. With the known diffusing-limiting and measured currents from the polarization curves, the kinetic currents were obtained according to the Koutecky-Levich equation [54]. For each catalyst, the calculated kinetic currents at 0.9 and 0.85 V were normalized to the mass

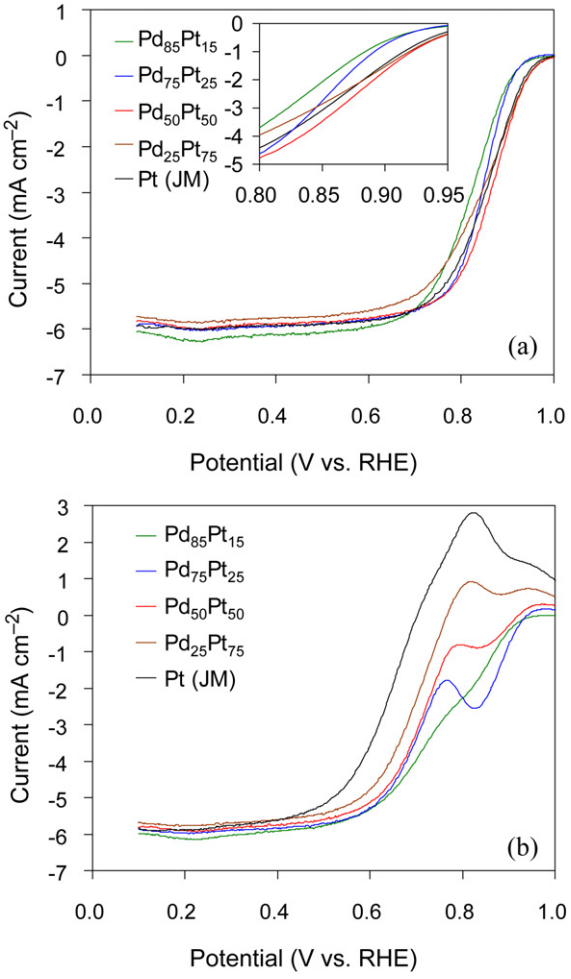

Fig. 9. Hydrodynamic polarization curves of PdPtCu/C samples with different Pd/Pt molar ratios and commercial Pt/C (JM) in O_2 saturated (a) 0.1 M $HClO_4$ and (b) a solution of 0.1 M $HClO_4$ and 0.1 M methanol at room temperature with a scan rate of 20 mV s^{-1} from 0.1 to 1.0 V vs. RHE.

Table 1
Percentages and mass activities toward ORR of the PdPtCu/C samples with different Pd/Pt molar ratios and Pt/C (40 wt%, JM).

Catalyst	wt%			0.90 V vs. RHE		0.85 V vs. RHE	
	Pd	Pt	Cu	$A/mg_{(Pt+Pd)}$	A/mg_{Pt}	$A/mg_{(Pt+Pd)}$	A/mg_{Pt}
PdPtCu/C-$Pd_{85}Pt_{15}$	22.5	7.3	1.4	0.04	0.15	0.18	0.72
PdPtCu/C-$Pd_{75}Pt_{25}$	19.7	10.9	1.3	0.05	0.12	0.28	0.78
PdPtCu/C-$Pd_{50}Pt_{50}$	13.6	19.6	1.8	0.11	0.19	0.43	0.73
PdPtCu/C-$Pd_{25}Pt_{75}$	6.1	26.9	3.3	0.10	0.13	0.29	0.35
Pt/C (JM)	n/a	40	n/a	N/A	0.08	N/A	0.25

to obtain the mass activities. With negligible particle size effects for the PdPtCu/C catalysts mentioned in Section 3.1, the mass activities can represent the intrinsic activities for comparison.

The obtained mass activities or the intrinsic activities are listed in Table 1, from which we can see that all the PdPtCu/C catalysts have higher Pt-based mass activities than Pt/C (JM). However, as for the noble metal (Pd and Pt) based activities, not all the catalysts show higher activities than Pt/C (JM). The ORR noble metal based activity decreases in the order PdPtCu/C-$Pd_{50}Pt_{50}$ ≈ PdPtCu/C-$Pd_{25}Pt_{75}$ > Pt/C (JM) > PdPtCu/C-$Pd_{75}Pt_{25}$ ≈ PdPtCu/C-$Pd_{85}Pt_{15}$ at 0.9 V, and PdPtCu/C-$Pd_{50}Pt_{50}$ > Pt/C (JM) ≈ PdPtCu/C-$Pd_{85}Pt_{15}$ ≈ PdPtCu/C-$Pd_{75}Pt_{25}$ ≈ PdPtCu/C-$Pd_{25}Pt_{75}$ at 0.85 V. It needs to be pointed out that the ORR activity of PdPtCu/C-$Pd_{50}Pt_{50}$ is 2 and 3 times that of the Pt/C (JM) with the same mass of noble metal and Pt, respectively, at 0.85 V. Moreover, although PdPtCu/C-$Pd_{85}Pt_{15}$, PdPtCu/C-$Pd_{75}Pt_{25}$, and PdPtCu/C-$Pd_{25}Pt_{75}$ have the similar noble metal based activities as Pt/C (JM), the alloy of Pd–Pt still has positive synergistic effects on the activity toward ORR when considering the lower activity of Pd. The enhanced intrinsic activity toward ORR is ascribed to the synergistic effects: ensemble [19], ligand [19], and strain [20], from the optimal composition and structure [55,56].

Fig. 9b compares the methanol tolerances of the PdPtCu/C catalysts. ORR has a cathodic current, which is defined as negative in this study. The higher the activity toward ORR a catalyst has, the larger negative current it produces. In the presence of methanol, the MOR catalyzed by Pt generates an anodic current, which is positive and counteracts the cathodic current of ORR. It can be confirmed that all catalysts, except PdPtCu/C-$Pd_{85}Pt_{15}$, have a turnover point where the current changes from negative to positive, indicating that electrochemical oxidation reactions (methanol oxidation reaction in this study) dominate the current generation. This means that a catalyst with a turnover point at a more positive potential has better methanol tolerance. Certainly, PdPtCu/C-$Pd_{85}Pt_{15}$ without a turnover point in the range of potential cycling has the best methanol tolerance. The turnover points are located at 0.70, 0.77, 0.92, and 0.93 V, respectively, for Pt/C (JM), PdPtCu/C-$Pd_{25}Pt_{75}$, PdPtCu/C-$Pd_{50}Pt_{50}$, and PdPtCu/C-$Pd_{75}Pt_{25}$. The turnover points increase in potential as the Pd content increases, representing a composition-dependent methanol tolerance. Above these points, the catalysts actually become anode catalysts.

The composition dependence of methanol tolerance can also be derived from the changes of the peaks shown in the hydrodynamic polarization curves in Fig. 9b. Pt/C (JM), PdPtCu/C-$Pd_{25}Pt_{75}$, PdPtCu/C-$Pd_{50}Pt_{50}$, and PdPtCu/C-$Pd_{75}Pt_{25}$ show a significant peak related to methanol oxidation, located at 0.83, 0.82, 0.80, and 0.77 V, respectively. As the Pd content increases, the peaks shift to lower potentials and the intensities decrease, indicating that the activities toward MOR decrease. As we know, Pd promotes the activity of Pt toward MOR at the anode of DMFC by removing the CO intermediates of MOR on Pt [3–6]. This opposing behavior could be attributed to the higher overpotentials for MOR and in the presences of O_2 in the cathode, with which the MOR intermediates oxidization rate could be very fast on Pt and the promotion effect from the addition of Pd can be negligible.

3.4. MEA performance and durability testing in a single cell configuration

As discussed in section 3.3, PdPtCu/C-$Pd_{50}Pt_{50}$ is the most promising cathode catalyst among the samples owing to the improved ORR activity and methanol tolerance compared to Pt/C (JM) in an electrochemical cell. To confirm the superior performance under actual DMFC conditions, PdPtCu/C-$Pd_{50}Pt_{50}$ was tested in a DMFC single cell. Fig. 10 compares the iR-free polarization curves of two MEAs with Pt/C (JM) and PdPtCu/C-$Pd_{50}Pt_{50}$ as the cathode catalysts in a DMFC single cell. The polarization curves show that the MEA with PdPtCu/C-$Pd_{50}Pt_{50}$ has superior performance than the Pt/C (JM) MEA above 0.25 V. This is mainly accredited to the higher methanol tolerance of PdPtCu/C-$Pd_{50}Pt_{50}$ compared to Pt/C (JM) as shown in Fig. 9b. It can be easily observed that the superiority decreases as the cell voltage decreases. The decrease in the cell voltage implies that the potential of the cathode decreases, leading to a lower MOR overpotential at the cathode. Therefore, less MOR current is generated at the cathode to counteract the ORR current and thus the PdPtCu/C-$Pd_{50}Pt_{50}$ MEA exhibits less improvement than the Pt/C (JM) MEA.

Fig. 11 shows the 180 h durability test of the PdPtCu/C-$Pd_{50}Pt_{50}$ and Pt/C (JM) MEAs in a DMFC single cell in galvanostatic mode at a current of 100 mA cm^{-2}. The voltage of both MEAs decreased remarkably during the first 50 h and then remained relatively stable. It is consistent with the observation from other researchers of the MEA with a commercial Pt/C catalyst [57]. The faster degradation rate in the beginning might be attributed to the equilibrium of the concentration gradient of the reactants in the MEA, as well as the poisoning from the intermediates of the methanol oxidation [57]. The historical conditions of the MEA could also affect the initial degradation rate, i.e., the rate of the first 50 h section. After which, the MEA is subjected to the degradation of structure and composition of the materials. The PdPtCu/C-$Pd_{50}Pt_{50}$ MEA exhibits a degradation rate of 38 μV/h after 50 h, which is much lower than

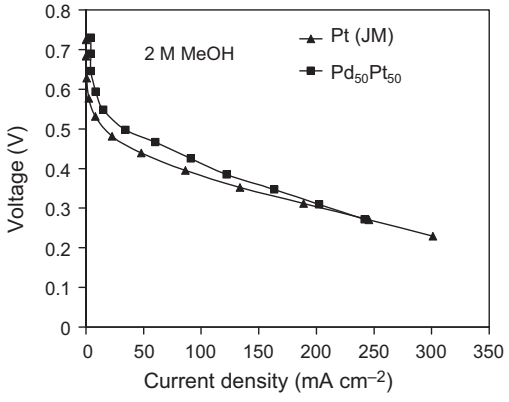

Fig. 10. iR-free polarization curves of Pt/C (JM) and PdPtCu/C-$Pd_{50}Pt_{50}$ tested in a DMFC single cell.

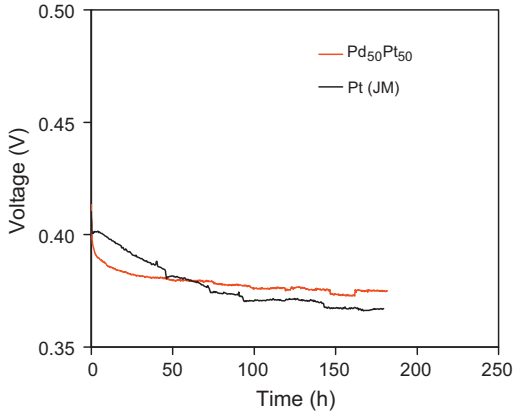

Fig. 11. Degradation curves of the PdPtCu/C-$Pd_{50}Pt_{50}$ and Pt/C (JM) MEAs under a constant current density of 100 mA cm^{-2}.

the 220 μV/h degradation of the Pt/C MEA during 50–100 h and a little lower than the 50 μV/h degradation of the Pt/C MEA after 100 h. The degradation rates of the Pt/C MEA are consistent with the reports in the literature [57–59]. One of the main proposed degradation factors is Ru from the PtRu NPs at the anode undergoing dissolution and transferring to the cathode leading to a decline in MEA performance [57,58]. Similarly, the base metal, such as Cu, in the cathode catalysts might leach from the alloy NPs and diffuse into the membrane to reduce the conductivity and also reach to the anode to contaminate the anode catalyst. The good stability of the MEA with PdPtCu/C-$Pd_{50}Pt_{50}$ prepared in this study suggests that the residual Cu does not have a substantial negative effect on the degradation. It also confirms that the Cu is beneath the surface of the PdPt alloy after etching in the reaction solution.

4. Conclusions

We have demonstrated the heterogeneous synthesis of highly dispersed and PdPt surface enriched PdPtCu alloy nanoparticles (NPs) on carbon support (PdPtCu/C) by using Cu NPs as a heterogeneous reducing agent. The experimental results showed that Cu NPs are an effective heterogeneous reducing agent for the formation of PdPtCu alloys, and the interplay existing between the noble metal precursors and the surface atoms of the Cu NPs contribute to the high dispersion of the alloy NPs as well as their uniform distribution on the carbon black. Moreover, the Pd/Pt molar ratio is tunable over the entire composition range with this synthesis route, which yields diverse catalytic activities based on the varied composition. The etching capability of the reaction solution after the production of the Cu NPs is switchable by controlling the atmospheric environment, i.e., under a N_2 atmosphere, the Cu NPs are stable and used to prepare the PdPtCu alloy NPs; under an air atmosphere, the Cu NPs in the surface layer of the PdPtCu NPs are removed by etching effects to construct the surface enrichment of PdPt. Finally, the prepared PdPtCu/C catalysts exhibit composition-dependent activities toward ORR and methanol tolerances. The PdPtCu/C with a Pd/Pt molar ratio of 1:1 has noble metal and Pt mass activities, respectively, 2 and 3 times that of a commercial Pt/C at 0.85 V vs. RHE as well as much superior methanol tolerance. This synthesis route is very facile and suitable for large-scale production. It can be used to prepare the PdPt surface enriched PdPtCu/C with different compositions for other reactions in LTFCs, such as HOR, MOR, EOR, FAOR, etc. It is anticipated that this synthesis route could become applicable for the preparation of other supported heterogeneous catalysts, such as PdPtCu/Al_2O_3, PtAuCu/C, etc.

Acknowledgements

This work was supported by the Office of Naval Research MURI grant no. N00014-07-1-0758 and Welch Foundation grant F-1254.\

Appendix A. Supplementary data

Supplementary data associated with this article can be found, in the online version, at http://dx.doi.org/10.1016/j.apcatb.2012.09.044.

References

[1] W. Vielstich, A. Lamm, H.A. Gasteiger (Eds.), Handbook of Fuel Cells: Fundamentals, Technology, Applications, Wiley, New York, 2003.
[2] S. Minhua, Journal of Power Sources 196 (2011) 2433–2444.
[3] F. Alcaide, G. Álvarez, P.L. Cabot, H.-J. Grande, O. Miguel, A. Querejeta, International Journal of Hydrogen Energy 36 (2011) 4432–4439.
[4] Y. Liu, M. Chi, V. Mazumder, K.L. More, S. Soled, J.D. Henao, S. Sun, Chemistry of Materials 23 (2011) 4199–4203.
[5] F. Kadirgan, S. Beyhan, T. Atilan, International Journal of Hydrogen Energy 34 (2009) 4312–4320.
[6] Y.-W. Lee, A.R. Ko, S.-B. Han, H.-S. Kim, K.-W. Park, Physical Chemistry Chemical Physics 13 (2011) 5569–5572.
[7] S.-C. Lin, J.-Y. Chen, Y.-F. Hsieh, P.-W. Wu, Materials Letters 65 (2011) 215–218.
[8] J. Lu, S. Lu, D. Wang, M. Yang, Z. Liu, C. Xu, S.P. Jiang, Electrochimica Acta 54 (2009) 5486–5491.
[9] X. Li, I.M. Hsing, Electrochimica Acta 51 (2006) 3477–3483.
[10] Y.N. Wu, S.J. Liao, Y.L. Su, J.H. Zeng, D. Dang, Journal of Power Sources 195 (2010) 6459–6462.
[11] C. Rice, S. Ha, R.I. Masel, A. Wieckowski, Journal of Power Sources 115 (2003) 229–235.
[12] E.A. Baranova, N. Miles, P.H.J. Mercier, Y. Le Page, B. Patarachao, Electrochimica Acta 55 (2010) 8182–8188.
[13] H.-X. Zhang, C. Wang, J.-Y. Wang, J.-J. Zhai, W.-B. Cai, Journal of Physical Chemistry C 114 (2010) 6446–6451.
[14] J. Liu, J. Ye, C. Xu, S.P. Jiang, Y. Tong, Electrochemistry Communications 9 (2007) 2334–2339.
[15] F. Alcaide, G. Álvarez, P.L. Cabot, O. Miguel, A. Querejeta, International Journal of Hydrogen Energy 35 (2010) 11634–11641.
[16] X. Li, Y. Zhu, Z. Zou, M. Zhao, Z. Li, Q. Zhou, D.L. Akins, H. Yang, Journal of the Electrochemical Society 156 (2009) B1107–B1111.
[17] A. Maghsodi, M.R. Milani Hoseini, M. Dehghani Mobarakeh, M. Kheirmand, L. Samiee, F. Shoghi, M. Kameli, Applied Surface Science 257 (2011) 6353–6357.
[18] H. Naohara, Y. Okamoto, N. Toshima, Journal of Power Sources 196 (2011) 7510–7513.
[19] P. Liu, J.K. Nørskov, Physical Chemistry Chemical Physics 3 (2001) 3814–3818.
[20] M. Mavrikakis, B. Hammer, J.K. Nørskov, Physical Review Letters 81 (1998) 2819–2822.
[21] N.M. Marković, P.N. Ross Jr., Surface Science Reports 45 (2002) 117–229.
[22] H. Wang, R. Wang, H. Li, Q. Wang, J. Kang, Z. Lei, International Journal of Hydrogen Energy 36 (2011) 839–848.
[23] R. Wang, H. Li, H. Feng, H. Wang, Z. Lei, Journal of Power Sources 195 (2010) 1099–1102.
[24] P. Strasser, S. Koh, T. Anniyev, J. Greeley, K. More, C. Yu, Z. Liu, S. Kaya, D. Nordlund, H. Ogasawara, M.F. Toney, A. Nilsson, Nature Chemistry 2 (2010) 454–460.
[25] M. Shao, K. Shoemaker, A. Peles, K. Kaneko, L. Protsailo, Journal of the American Chemical Society 132 (2010) 9253–9255.
[26] R. Wang, Z. Zhang, H. Wang, Z. Lei, Electrochemistry Communications 11 (2009) 1089–1091.
[27] M. Brust, M. Walker, D. Bethell, D.J. Schiffrin, R. Whyman, Journal of the Chemical Society, Chemical Communications (1994) 801–802.
[28] J. Luo, M.M. Maye, N.N. Kariuki, L. Wang, P. Njoki, Y. Lin, M. Schadt, H.R. Naslund, C.-J. Zhong, Catalysis Today 99 (2005) 291–297.
[29] M. Maye, N. Kariuki, J. Luo, L. Han, P. Njoki, L. Wang, Y. Lin, H. Naslund, C.-J. Zhong, Gold Bulletin 37 (2004) 217–223.
[30] M.J. Hostetler, C.-J. Zhong, B.K.H. Yen, J. Anderegg, S.M. Gross, N.D. Evans, M. Porter, R.W. Murray, Journal of the American Chemical Society 120 (1998) 9396–9397.
[31] C. Wu, B.P. Mosher, T. Zeng, Chemistry of Materials 18 (2006) 2925–2928.
[32] C. Wu, T. Zeng, Chemistry of Materials 19 (2006) 123–125.
[33] X. Wen, Y.-T. Xie, W.C. Mak, K.Y. Cheung, X.-Y. Li, R. Renneberg, S. Yang, Langmuir 22 (2006) 4836–4842.
[34] B.L. Garc'ia, J.W. Weidner, R.E. White, C.G. Vayenas, M.E. Gamboa-Aldeco, in: R.E. White, C.G. Vayenas (Eds.), Modern Aspects of Electrochemistry, vol. 40, Springer, New York, 2007, pp. 229–284.
[35] A.K. Shukla, R.K. Raman, Annual Review of Materials Research 33 (2003) 155–168.
[36] X. Zhao, W. Li, A. Manthiram, Journal of Power Sources 201 (2011) 37–42.
[37] P. Vanýsek, in: D.R. Lide (Ed.), CRC Handbook of Chemistry and Physics, 81st ed., CRC Press LLC, Roca Raton, 2000/2001, pp. 8-21–8-28.

[38] W.R. Tyson, W.A. Miller, Surface Science 62 (1977) 267–276.
[39] A.O. Dekker, R.G. Dickinson, Journal of the American Chemical Society 62 (1940) 2165–2171.
[40] E.V. Shtamm, A.P. Purmal, Y.I. Skurlatov, International Journal of Chemical Kinetics 11 (1979) 461–494.
[41] C.W. Shih, Y.Y. Wang, C.C. Wan, Journal of Applied Electrochemistry 32 (2002) 987–992.
[42] O. Çakır, H. Temel, M. Kiyak, Journal of Materials Processing Technology 162–163 (2005) 275–279.
[43] L.K. Ono, J.R. Croy, H. Heinrich, B. Roldan Cuenya, Journal of Physical Chemistry C 115 (2011) 6856–16866.
[44] M.W. Breiter, Journal of Electroanalytical Chemistry and Interfacial Electrochemistry 81 (1977) 275–284.
[45] T. Mallát, É. Polyánszky, J. Petró, Journal of Catalysis 44 (1976) 345–351.
[46] C.-C. Hu, T.-C. Wen, Journal of the Electrochemical Society 142 (1995) 1376–1383.
[47] J. Clavilier, Journal of Electroanalytical Chemistry and Interfacial Electrochemistry 107 (1979) 211–216.
[48] B.E. Conway, Progress in Surface Science 49 (1995) 331–452.
[49] H. Angerstein-Kozlowska, B.E. Conway, W.B.A. Sharp, Journal of Electroanalytical Chemistry and Interfacial Electrochemistry 43 (1973) 9–36.
[50] B.V. Tilak, B.E. Conway, H. Angerstein-Kozlowska, Journal of Electroanalytical Chemistry and Interfacial Electrochemistry 48 (1973) 1–23.
[51] L.H. Dall'Antonia, G. Tremiliosi-Filho, G. Jerkiewicz, Journal of Electroanalytical Chemistry 502 (2001) 72–81.
[52] M. Grdeń, M. Łukaszewski, G. Jerkiewicz, A. Czerwiński, Electrochimica Acta 53 (2008) 7583–7598.
[53] J.J. Chen, E. Ruckenstein, Journal of Physical Chemistry 85 (1981) 1606–1612.
[54] A.J. Bard, L.R. Faulkner, Electrochemical Methods: Fundamentals and Applications, second ed., Wiley, New York, 2001.
[55] H. Li, G. Sun, N. Li, S. Sun, D. Su, Q. Xin, Journal of Physical Chemistry C 111 (2007) 5605–5617.
[56] J. Zhang, Y. Mo, M.B. Vukmirovic, R. Klie, K. Sasaki, R.R. Adzic, Journal of Physical Chemistry B 108 (2004) 10955–10964.
[57] X. Cheng, C. Peng, M. You, L. Liu, Y. Zhang, Q. Fan, Electrochimica Acta 51 (2006) 4620–4625.
[58] S.D. Knights, K.M. Colbow, J. St-Pierre, D.P. Wilkinson, Journal of Power Sources 127 (2004) 127–134.
[59] C.-Y. Chen, H.-C. Cha, Journal of Power Sources 200 (2012) 21–28.